Precise Measurements of the Q Factor of Dielectric Resonators in the Transmission Mode—Accounting for Noise, Crosstalk, Delay of Uncalibrated Lines, Coupling Loss, and Coupling Reactance

Kenneth Leong, *Member, IEEE*, and Janina Mazierska, *Senior Member, IEEE*

***Abstract*—Accurate measurements of the unloaded Q_o factor of microwave resonators are necessary in many microwave applications. The most accurate values of Q_o can be obtained by Q-circle fits from multifrequency S-parameter data. Practical measurement systems cause S-parameters of the resonators to be distorted from the circular ideal shape, rotated, and shifted from the origin resulting in errors in the Q-factor values. A novel Q-factor measurement method has been developed based on equations derived for resonators working in the transmission mode and fractional linear circle-fitting techniques. The transmission-mode Q-factor (TMQF) technique removes measurement effects of noise, noncalibrated measurement cables, connectors, coupling structures, crosstalk between the coupling loops, and impedance mismatch from the measurement data. The TMQF is especially useful in cryogenic measurements of high-temperature-superconductor thin films and dielectrics since these measurements are typically done in the transmission mode and contain cables and connectors that are difficult to calibrate. The accuracy of the TMQF is better than 1% for practical measurement ranges and the method is applicable to a wide range of coupling. The range of Q factors measurable is from 10^3 up to 10^7.**

***Index Terms*—Dielectric resonators, measurements effects, S-parameters, transmission-mode measurements, TMQF, unloaded Q factor.**

I. Introduction

MEASUREMENTS of the unloaded Q_o factor play an important role in the assessment of performance of systems and material properties. The Q-factor values are especially useful in measurements of selectivity of systems, as well as surface resistance of conducting and superconducting materials and complex permittivity of dielectric materials [1]–[3].

By definition, the quality factor is a ratio of the maximum energy $W_{\max}$ stored within a system to the energy dissipated W_d by this system [4] as follows:

$$Q = \frac{2\pi W_{\max}}{W_d}.$$

Manuscript received July 9, 2001. This work was supported by James Cook University under ARC Large Grant A498802435 and Grant A0799.

K. Leong was with the Electrical and Computer Engineering, James Cook University, Townsville, Qld. 4811, Australia. He is now with the Electromagnetic Technology Division, National Institute of Standards and Technology, Boulder, CO 80305-3328 USA.

J. Mazierska is with the Electrical and Computer Engineering, James Cook University, Townsville, Qld. 4811, Australia.

Publisher Item Identifier 10.1109/TMTT.2002.802324.

The unloaded Q_o factor of the system is obtained from the measured loaded Q_L factor of this system together with external circuitry and coupling coefficients. For resonators in the transmission mode $Q_o = Q_L(1 + \beta_1 + \beta_2)$, where the coupling coefficients β_1 and β_2 are defined as a ratio of the external power dissipated to power dissipated in the system. For resonators working in the reflection mode $Q_o = Q_L(1 + \beta)$.

Under a very weak coupling condition, the unloaded Q_o factor can be approximated by the loaded Q_L factor ($Q_o \approx Q_L$), eliminating the need for β measurements. However, measurements with low coupling usually result in low SNR ratio that may affect the accuracy of the measurements. Hence, it is desirable to use sufficiently high levels of coupling.

Methods used to obtain the loaded Q_L factor and β are based on measurements of various types of system response: impedance [5], [6], power [5], [7]–[10], voltage standing-wave ratio (VSWR) [5] and S-parameters [4], [11]–[15]. Measurements of a chosen response are done either in the frequency or time domains. Although the 3-dB "three frequencies" method is used often to determine Q_L, the most accurate results are obtained by fitting a circle to multifrequency data. This is a more accurate method than the 3-dB method because all points around the resonance contribute to the definition of the circle. While the multifrequency tests were very time consuming when first proposed by Gintzon [5], with the availability of vector network analyzers, they should become a standard practice for accurate measurements.

Most of the Q-factor measurement techniques have been developed based on ideal models of resonator systems. Hence, any discrepancy between the ideal resonator and practical resonator measurement system and inadequacies of calibration procedures result in errors in measured Q-factor values, as illustrated in Section II. Recently, there has been strong interest in precise microwave characterization of new (and some "old") materials at cryogenic temperatures for applications to wireless communications. Most cryogenic measurement systems contain cables and adaptors, which cannot easily (if ever) be calibrated. Hence, a new and accurate Q-factor measurement method was needed, which accounts for parasitic measurement effects (noise, noncalibrated cables, connectors, coupling structures, crosstalk, and impedance mismatch) and this is the goal of this paper.

An existing method [4] accounts for some of the mentioned effects, but is applicable to the reflection mode resonators only.

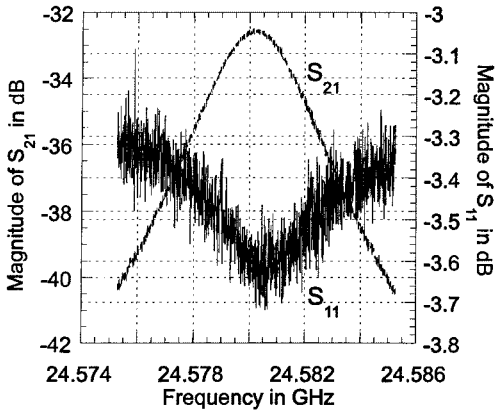

Fig. 1. Magnitude traces of S_{21} and S_{11} for a resonator with $f_{\rm res} = 24.58$ GHz, $Q_L = 5564$, $S_{21\,\max} = -32.6$ dB, BW $= 4.42$ MHz, and span $= 10$ MHz.

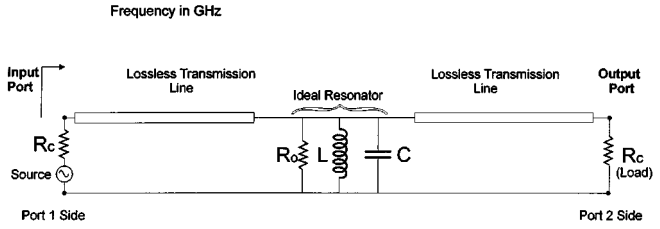

Fig. 2. Circuit model of a measurement system based on a dielectric resonator.

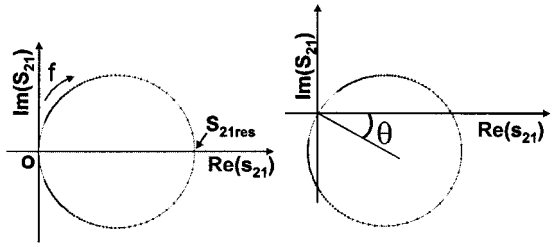

(a) (b)

Fig. 3. Q circle. (a) Ideal. (b) With delay due to transmission lines.

As mentioned earlier, most of microwave characterization of materials is usually done in the transmission mode due to a much higher SNR ratio.

II. Review of Effects Introduced by the Measurement System on the Dielectric-Resonator Response

The development of an accurate curve-fitting technique to obtain the unloaded Q_o factor of microwave resonators requires a good understanding of practical effects introduced by real measurement systems. The S-parameters of an ideal resonator measured near the resonance should form circles in the complex plane centered at the origin. However, due to effects associated with external measurement circuitry, the measured responses of a dielectric resonator are distorted from their ideal circular shape and often do not pass through the origin of the complex plane. Phenomena that may affect the S-parameters of dielectric resonators are: 1) noise; 2) electrical delay introduced by transmission lines; 3) losses due to transmission lines; 4) connectors; 5) coupling structures; 6) impedance mismatch; and 6) crosstalk between the coupling loops of transmission-mode resonators. Identified phenomena [16] are documented and discussed below.

A. Effects of Noise

Noise is always present in any measurement data as random variations of amplitude and phase caused by thermal effects, instabilities in microwave sources, and vibrations of a resonator. Under weak coupling conditions, the noise in a reflection trace is usually significantly higher than in the transmission trace. Fig. 1 shows the S_{21}- and S_{11}-parameters measured using the same coupling ($S_{21\,\max} = -32.6\ dB$) on the input and output ports for a Hakki–Coleman sapphire resonator in a copper cavity resonating at 24.58 GHz at room temperature with the loaded Q_L factor of 5564. The S_{21} magnitude trace averaged over 16 sweeps is well defined, but the S_{11} magnitude trace is clearly much more noisy.

When curve-fitting procedures are applied to raw measurement data, the effect of noise can be eliminated to a large extent. However, a low SNR ratio can affect the accuracy of the fitting techniques, especially when the amount of noise exceeds a certain limit [4]. This is why transmission-mode measurements are often used instead of the reflection mode, as the SNR is usually high enough for curve-fitting techniques to be applied accurately.

B. Effects of Electrical Delay Introduced by Uncalibrated Transmission Lines on the Measured Characteristics of Dielectric Resonators

Consider a circuit model of an ideal transmission-mode resonator modeled by parallel *RLC* elements together with lossless transmission lines connecting the resonator to a microwave source and a load, as shown in Fig. 2. Uncalibrated transmission lines introduce a frequency-dependent electrical delay, equivalent to a frequency-dependent phase shift [4], $\phi(f) = \phi_{\rm ref} f/f_{\rm ref}$, where $\phi_{\rm ref}$ is the phase introduced by the transmission line at the arbitrary reference frequency $f_{\rm ref}$. If the length of the transmission lines in the measurement system is zero, the $S_{21}Q$ circle of the system passes through the origin and is centered on the real axis, as shown schematically in Fig. 3(a). The detuned point, which represents a point at a frequency far away from the resonance, lies at the origin in this case. For any nonzero length of the transmission lines, an electrical delay is introduced and causes all the points on the ideal Q circle to be rotated about the origin. The rotation angle θ depends on the length of transmission line [see Fig. 3(b)].

Rotation of each point on the Q circle in Fig. 3 is frequency dependent. This phenomenon is illustrated in Fig. 4 showing the phase of the S_{11}-parameter changing linearly due to frequency dependence of the delay introduced by transmission lines. Measurements shown in Fig. 4 were made with a 25-GHz sapphire resonator in the copper cavity at room temperature exhibiting Q_L of 2574 for $S_{21\,\max}$ of -8.1 dB. The irregularity at the mid-span is due to phase characteristics of the microwave resonator at the resonance.

The frequency dependence of the phase shift causes larger rotation of points on the Q circle at higher frequencies in the

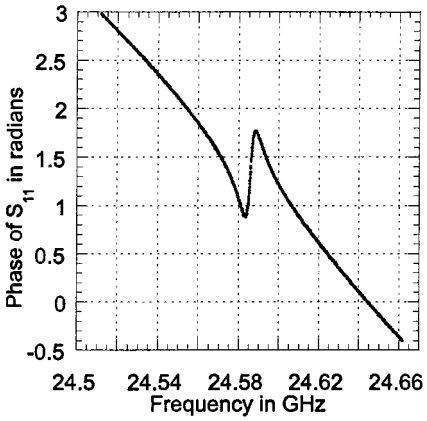

Fig. 4. Phase of S_{11} trace versus frequency for the resonator with $Q_L = 2574$, uncalibrated cables of 40 cm per cable, $f_{\rm res} = 24.59$ GHz, span $= 150$ MHz, and BW $= 4.42$ MHz.

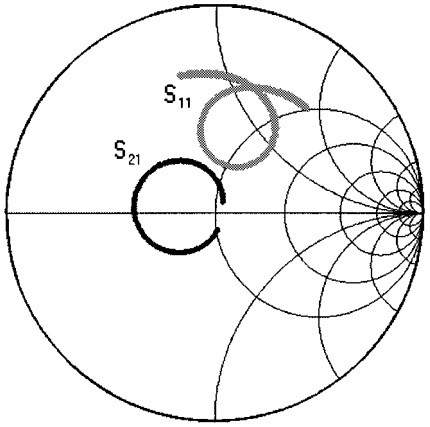

Fig. 5. Measured "balloon"-shaped reflection S_{11} Q circle and the transmission S_{21} Q circle for the resonator with $Q_L = 2574$, $S_{21\,\max} = -8.1$ dB, $f_{\rm res} = 24.59$ GHz, BW $= 9.55$ MHz, and span $= 50$ MHz, and cable length of 40 cm on each port.

complex frequency plane than the rotation of points at lower frequencies. As a result, a distortion of the circular shape of the Q circle to a "balloon" shape occurs. This phenomenon is illustrated in Fig. 5 for the S_{11} Q circle of the dielectric resonator with Q_L of 2574 and $S_{21\,\max}$ of -8.1 dB. The transmission S_{21} Q circle measured for the same case (also shown in Fig. 5) is significantly less distorted.

Cables connecting a dielectric resonator to the measurement system also introduce attenuation of microwave signals. The effect of attenuation on a reflection (S_{11} or S_{22}) Q circle is a reduction in the diameter, as well as a movement away from the unit circle on the Smith Chart. Effects of loss introduced by coupling and system elements are discussed in Section II-D.

C. Effects of Impedance Mismatch

Impedance mismatch between sections of a measurement system causes reflections of microwave signals at mismatched points. For a matched system, the center of the circular S_{11} or S_{22} trace observed in off-resonance regions (for frequencies far from the resonance) is expected to lie at the origin of the Smith Chart. However, we observed a noticeable offset of the center of the off-resonance traces of S_{11} and S_{22} from the origin in

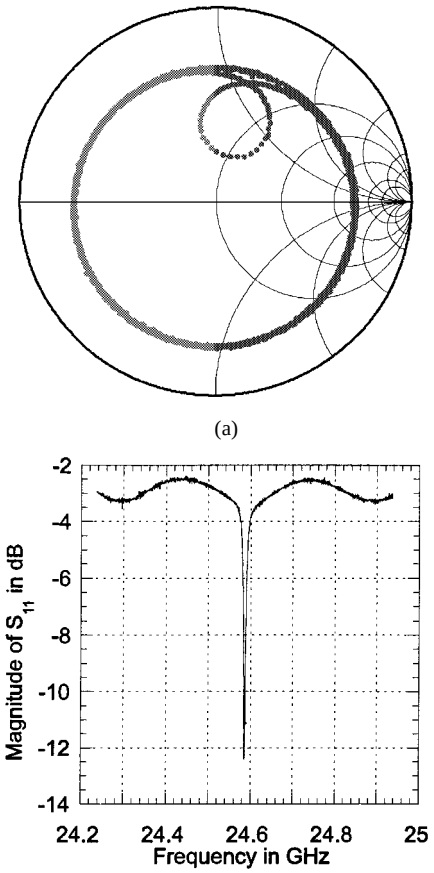

Fig. 6. Observed mismatch effect in the S_{11}. (a) Resonance Q circle and the off-resonance circle. (b) Magnitude trace for the resonator with $Q_L = 2574$, $S_{21\,\max} = -8.1$ dB, $f_{\rm res} = 24.59$ GHz, and span $= 400$ MHz.

the wide-band measurements. Fig. 6(a) presents a mismatch effect observed in the off-resonance part of the reflection S_{11} trace of the 25-GHz sapphire resonator in the copper cavity at room temperature. The S_{11} Q circle (which is evidently distorted due to transmission-line phase effects, as discussed in Section II-B) is attached to the larger off-resonance circle. The center of the off-resonance circle clearly does not coincide with the center of the Smith Circle, indicating the presence of impedance mismatch.

The effect of impedance mismatch can be observed clearly in the magnitude trace of reflection response. If mismatch is not present, then the magnitude of the response in the off-resonance region is at a constant level. In the presence of mismatch, the magnitude of S_{11} changes periodically with frequency, except at the resonance peak, as shown in Fig. 6(b).

The offset of the center of the off-resonance trace from the origin due to mismatch also causes a nonlinear effect in the phase of reflection response S_{11} and S_{22}. If there were no mismatch and, therefore, no offset of the center of the off-resonance circle from the origin, then a periodic linear phase response is expected, with the phase of each linear section going from $+\pi$ to $-\pi$ rad. With the mismatch present, the phase response deviates from a straight line. This is illustrated in Fig. 7, showing the mismatch effect on the phase of S_{11} for the resonator under the same conditions as in Fig. 6(a). The small irregularity in the phase at mid-span is associated with the resonance.

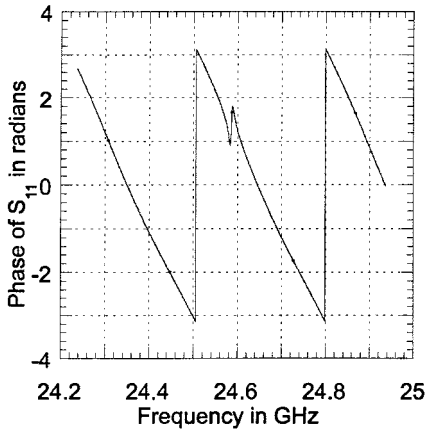

Fig. 7. Phase of the S_{11} response for the resonator with $Q_L = 2574$, $S_{21\max} = -8.1$ dB, $f_{\rm res} = 24.59$ GHz, and span $= 400$ MHz.

The effect of the impedance mismatch is considered important because it can alter significantly both the magnitude and phase of the reflection S_{11} or S_{22} responses around the resonance. While this effect has not yet been investigated thoroughly, the frequency dependence of mismatches can be observed experimentally using a time-domain reflectometer.

D. Effects of Coupling Loss and Reactance on the Measured Characteristics of Dielectric Resonators

Coupling of a resonator to an external circuit usually alters measured responses of the resonator. Coupling structures are usually in the form of a coupling loop (or iris) and have finite resistances that contribute to the microwave losses in the system. Also, microwave energy is stored in the coupling structure and this phenomenon is usually modeled as a reactance that is frequency dependent. However, for high-Q-factor systems (when the bandwidth of measurements is very small), it may be justifiable to assume that the reactance is constant in the frequency band around the vicinity of the resonance [4].

Our measurements using Hakki–Coleman sapphire resonators in the copper cavity have shown that the frequency dependence of coupling reactances did not influence the magnitude of the off-resonance reflection traces. If the frequency dependence of the reactance were significant, then the reflection vector would have not followed the path of a perfect circle. The off-resonance S_{11} trace of Fig. 6(a) is clearly circular, indicating that the assumption of a constant coupling reactance is justified for the resonator with a loaded Q_L factor of about 2600. The assumption of the constant coupling becomes more accurate for higher Q_L factors, hence, there is no need to consider frequency dependence of coupling reactances for resonators with Q factors higher than 1000.

Coupling losses and coupling reactance effectively reduce the coupling to the resonator and decrease the diameter of S_{21} Q circles. The effect of coupling loss (and any other loss in the system) can be investigated by examining the location of the reflection mode (S_{11} or S_{22}) Q circles on the Smith chart complex plane. Fig. 8 shows simulated Q circles varying in size and position for different coupling loss.

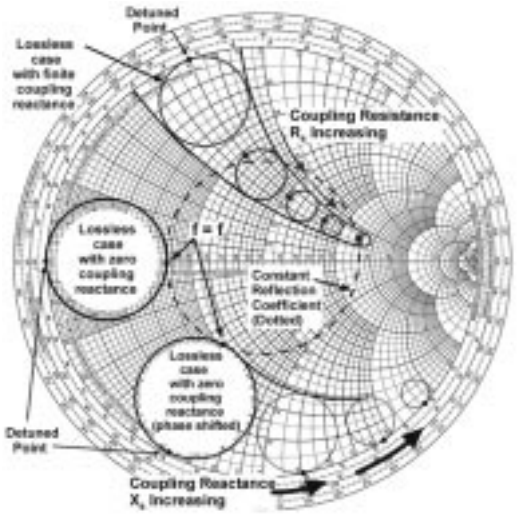

Fig. 8. Reflection Q circles for various cases of coupling loss and coupling reactance.

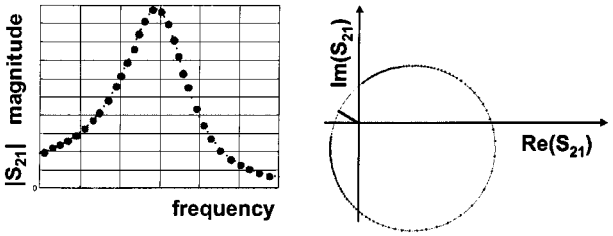

Fig. 9. Effect on crosstalk on S_{21} parameter. (a) Magnitude. (b) Q circle.

For a system with no coupling losses, but with a transmission-line delay, the reflection circle has the center on the real axis and the detuned point at $\Gamma = -1$ of the Smith circle. When coupling losses are present, the reflection Q circle no longer touches the circumference of the Smith circle. When the coupling reactance is held constant and the coupling losses are increased from zero, the Q circle moves away from the perimeter of the Smith circle with decreasing diameter, while all points on the circle maintain the same reactance. When the coupling losses are held constant and the coupling reactance is increased, the Q circle moves with decreasing diameter in the direction of the change in reactance with points moving along lines of constant resistance, as shown in Fig. 8.

E. Effects of Crosstalk

In the presence of crosstalk between the two ports of a resonator, the magnitude transmission response deviates from the perfect Lorentzian "bell shape," as illustrated in Fig. 9(a). However, the crosstalk does not distort the shape of the Q circles.

If no crosstalk is present, then the detuned point of the S_{21} circle lies at the origin. When crosstalk is present, the detuned point moves away from the origin [see Fig. 9(b)]. In the measurements shown in Fig. 5(b), the effect of crosstalk is clearly evident because a full circle fitted to the S_{21} trace would not pass through the origin.

TABLE I
POSSIBLE WAYS TO ACCOUNT FOR DISTORTION EFFECTS ON S-PARAMETERS OF DIELECTRIC RESONATORS

PARASITIC EFFECT	ACCOUNTING PROCEDURE
Noise (amplitude and phase)	Curve fitting
Coupling loss and reactance	Incorporation into a model
Transmission line loss and connector loss	Incorporation into a model
Crosstalk	Circle offset in curve fitting or incorporating into a model
Frequency dependant delay due to transmission lines	Calibration or a phase correction procedure

F. Summary—How to Deal With Effects Introduced by Real Measurement Systems on Characteristics of Dielectric Resonators

Measured S-parameters of dielectric resonators are distorted by noise, electrical delay introduced by transmission lines, losses due to uncalibrated transmission lines and coupling structures, impedance mismatch, and crosstalk. Some of the effects can be eliminated through a calibration procedure. Other distortions need to be removed from measured raw data through fitting procedures to obtain more accurate values of S-parameters and, thus, the loaded and unloaded Q factor of the resonator. A summary of possible ways of removing various distortions is presented in Table I.

III. TRANSMISSSION-MODE Q-FACTOR TECHNIQUE FOR ACCURATE DETERMINATION OF THE UNLOADED Q_o FACTOR OF MICROWAVE RESONATORS BASED ON MEASUREMENTS OF S-PARAMETERS

The following fundamental assumptions have been made to develop a feasible, accurate, and useful method to determine the Q_o factor of dielectric resonators.

1) The method is to be applicable to resonators working in the transmission mode.
2) The full equation to calculate the unloaded Q_o factor is to be used, namely,

$$Q_o = Q_L\,(1+\beta_1+\beta_2) \tag{1}$$

implying the following.
   a) A new equation is needed to relate the loaded Q_L factor with S_{21}-parameters around the resonance through a circuit model of the dielectric resonator system.
   b) A new equation in needed to relate coupling coefficients β_1 and β_2 with S_{11} and S_{22} reflection parameters for transmission-mode resonators.
3) Derivation of equations of the loaded Q_L factor, coupling coefficient, and frequency versus the S_{21} relationship is to be based on as accurate model of a real measurement system as feasible.
4) Important parasitic effects of a real resonator measurement system described in Section II, but not included in the circuit model of the system, are to be accounted for in the circle-fitting procedure applied to measured S-parameter responses of the system.

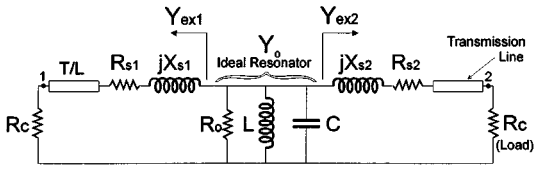

Fig. 10. Circuit model of a transmission resonator system.

To derive equations relating the S-parameters with the loaded Q_L factor, coupling coefficients, and the resonant frequency, the circuit model of a transmission-mode resonator illustrated in Fig. 10 has been used.

The three components R_o, L, and C of shunt admittance Y_o represent the ideal dielectric resonator. The shunt elements determine the unloaded Q_o factor of the system that can be described using a narrow-band approximation [1] as

$$Y_o = \frac{1}{R_o}\left\{1 + j2Q_o\frac{(\omega-\omega_o)}{\omega_o}\right\} \tag{2}$$

where Q_o is the unloaded quality factor of the resonator and the radian resonant frequency ω_o of the ideal resonator given by

$$\omega_o = \frac{1}{\sqrt{LC}}. \tag{3}$$

The admittances Y_{ex1} and Y_{ex2} denote external admittances seen on each port of the ideal resonator in Fig. 10 and are given by

$$y_{\text{exp}} = \frac{1}{R_{sp}+R_c+jX_{sp}} = G_{\text{exp}} + jB_{\text{exp}} \tag{4}$$

where p of 1 or 2 denotes the input and output port of the resonator respectively. Resistances R_{s1} and R_{s2} represent losses of coupling structures, connectors, and losses of transmission lines connected to two ports of the resonator; reactances of the coupling structures are modeled by X_{s1} and X_{s2}. The resistance R_c represents an internal resistance of a microwave source, a load resistance and characteristic impedance of transmission lines at both ports.

The circuit diagram of Fig. 10 can be considered as a cascaded connection of three networks and can be described using the $ABCD$ matrix as

$$\begin{bmatrix} A & B \\ C & D \end{bmatrix} = \begin{bmatrix} 1 & R_{s1}+jX_{s1} \\ 0 & 1 \end{bmatrix}\begin{bmatrix} 1 & 0 \\ Y_o & 1 \end{bmatrix}\begin{bmatrix} 1 & R_{s2}+jX_{s2} \\ 0 & 1 \end{bmatrix}. \tag{5}$$

Transmission lines have been treated as ideal and have not been included in (5). Their losses and delay are accounted for later.

The S-parameters of the total resonator system can be obtained from the $ABCD$-parameters using equations after [2], namely,

$$S_{21} = \frac{2R_c}{AR_c + B + CR_c^2 + DR_c} \tag{6}$$

$$S_{11} = \frac{(A-D)R_c + B - CR_c^2}{(A+D)R_c + B + CR_c^2} \tag{7}$$

$$S_{22} = \frac{(D-A)R_c + B - CR_c^2}{(A+D)R_c + B + CR_c^2}. \tag{8}$$

A. Derivation of Relationships Between Q_L and S_{21} (and S_{11} and S_{22})

Substituting (5) into (6), the following expression for the transmission coefficient S_{21} can be obtained as follows:

$$S_{21} = \frac{2R_c Y_{\text{ex1}} Y_{\text{ex2}}}{Y_{\text{ex1}} + Y_{\text{ex2}} + Y_o}. \tag{9}$$

The denominator of (9) is equal to the total admittance Y_L, where

$$\begin{aligned} Y_L &= Y_o + Y_{\text{ex1}} + Y_{\text{ex2}} \\ &= G_o + G_{\text{ex1}} + G_{\text{ex2}} + j2Q_o G_o \frac{\omega - \omega_o}{\omega_o} \\ &\quad + j\left(B_{\text{ex1}} + B_{\text{ex2}}\right). \end{aligned} \tag{10}$$

The resonant frequency ω_L[1] of the loaded resonator can be found from (10) assuming the imaginary part of the total admittance Y_L to be zero, namely,

$$\omega_L = \omega_o \left[1 - \frac{B_{\text{ex1}} + B_{\text{ex2}}}{2Q_o G_o}\right]. \tag{11}$$

On the basis of (9)–(11), the frequency dependence near the resonance of the complex transmission coefficient S_{21} for transmission-mode resonators can be expressed by a novel equation relating S_{21} with the loaded Q_L factor, coupling coefficients, and frequency

$$\begin{aligned} S_{21}(\omega) &= \frac{2R_c Y_{\text{ex1}} Y_{\text{ex2}}}{G_o(1+\beta_1+\beta_2)\left[1 + j2Q_L \dfrac{(\omega-\omega_L)}{\omega_o}\right]} \\ &\approx \frac{2R_c Y_{\text{ex1}} Y_{\text{ex2}}}{G_o(1+\beta_1+\beta_2)\left[1 + j2Q_L \dfrac{(\omega-\omega_L)}{\omega_L}\right]} \end{aligned} \tag{12}$$

where β_1 and β_2 are the coupling coefficients of the loaded resonator

$$\beta_1 = \frac{G_{\text{ex1}}}{G_o} \text{ and } \beta_2 = \frac{G_{\text{ex2}}}{G_o} \tag{13}$$

and Q_L is the Q factor of the loaded resonator

$$Q_L = Q_o \left(\frac{G_o}{G_o + G_{\text{ex1}} + G_{\text{ex2}}}\right). \tag{14}$$

[1]The loaded ω_L and unloaded ω_o resonant frequencies of the dielectric resonator have a similar meaning as the loaded and unloaded Q factors.

The approximation of $\omega_o \cong \omega_L$ can be considered acceptable for systems with high-Q factors. Equation (12) has a fractional linear form [4], sometimes called a bilinear form

$$S_{21} = \frac{a_1 t + a_2}{a_3 t + 1} \tag{15}$$

where the complex constants a_1, a_2, and a_3 are

$$a_1 = 0 \quad a_2 = \frac{2R_c Y_{\text{ex1}} Y_{\text{ex2}}}{G_o(1+\beta_1+\beta_2)} \quad a_3 = jQ_L \tag{16}$$

and "t" is a normalized frequency variable defined by

$$t = 2\left(\frac{\omega - \omega_L}{\omega_L}\right). \tag{17}$$

The parameter a_3, the imaginary part of which is equal to the loaded Q_L factor, namely,

$$Q_L = \text{Im}[a_3] \tag{18}$$

is obtained using a fractional linear curve-fitting procedure applied to (12). For completeness, the relationships between the reflection parameters S_{11} and S_{22} and the loaded Q_L factor have been obtained. Substitution of the (5)–(7) into (8) results in

$$\begin{aligned} S_{pp}(\omega) &= \frac{jQ_L S_{ppd} 2\dfrac{(\omega-\omega_L)}{\omega_L} + \left\{S_{ppd} + \dfrac{2R_c Y_{\text{exp}}^2}{G_o(1+\beta_1+\beta_2)}\right\}}{jQ_L 2\dfrac{(\omega-\omega_L)}{\omega_L} + 1} \end{aligned} \tag{19}$$

where S_{ppd} represents the detuned value of the reflection coefficient at the port p of 1 or 2 when the frequency is far from ω_L. Similarly to S_{21}, expressed by (12), (19) is also of the fractional linear form

$$S_{pp} = \frac{a_1 t + a_2}{a_3 t + 1} \tag{20}$$

and, hence, it is also suitable for a fractional linear curve-fitting technique. The complex constants in (20) are related to important points on the Q circles: the ratio a_1/a_3 represents the detuned value of the complex reflection coefficient S_{ppd}, a_2 is the reflection coefficient at the resonant frequency, and the imaginary part of a_3 is equal to Q_L, namely,

$$\begin{aligned} a_1 &= jQ_L S_{ppd} \\ a_2 &= S_{ppd} + \frac{2R_c Y_{\text{exp}}^2}{G_o(1+\beta_1+\beta_2)} \\ a_3 &= jQ_L. \end{aligned} \tag{21}$$

The complex constant a_3 is the same as for the transmission case solution, which means that Q_L for transmission-mode resonators can be found either from the transmission or the reflection responses. The diameter of reflection circles can be obtained from the detuned and resonance points, which lie diametrically opposite to each other on the Q circle.

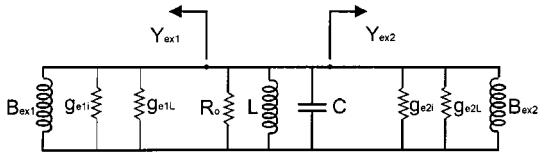

Fig. 11. Equivalent circuit of the transmission resonator to model coupling losses.

B. Derivation of a Relationship Between Coupling Coefficients β_1 and β_2 and S_{11} and S_{22}

Values of coupling coefficients of a transmission resonator system cannot be obtained directly from data sets of S_{11} and S_{22} measured near the resonant frequency. To solve the problem, we have employed a concept of splitting the coupling coefficients into two parts, i.e., lossless and lossy, applied before in [12] for the reflection-mode resonators. To model the coupling losses, we used the equivalent-circuit model shown in Fig. 11. The model of Fig. 11 is similar to the model a reflection mode (one-port) resonator in [4], but contains two ports. The coupling coefficient on each of the resonator ports can be expressed as

$$\beta_p = \frac{G_{\text{exp}}}{G_o} = \left(\frac{g_{epi}}{G_o}\right) + \left(\frac{g_{epL}}{G_o}\right) \tag{22}$$

where the external conductance G_{exp} is considered as the sum of the ideal lossless part g_{epi} and an additional lossy part g_{epL}. Hence, the total coupling coefficients can be considered as a sum of lossless β_i and lossy β_L terms, namely,

$$\beta_1 = \beta_{1i} + \beta_{1L} \text{ and } \beta_2 = \beta_{2i} + \beta_{2L} \tag{23}$$

where the lossless and lossy coupling coefficients are

$$\beta_{pi} = \frac{g_{epi}}{G_o} = \frac{R_o R_c}{(R_c + R_{sp})^2 + X_{sp}^2} \tag{24}$$

$$\beta_{pL} = \frac{g_{epL}}{G_o} = \frac{R_o R_{sp}}{(R_c + R_{sp})^2 + X_{sp}^2}. \tag{25}$$

For reflection-mode resonators, it has been shown [4] that the lossless and lossy parts of the coupling coefficient can be calculated from the diameter of the reflection Q circle and the diameter of the *coupling-loss* circle. We have obtained β_{pi} and β_{pL} terms for the transmission-mode resonators using the same geometrical approach, but solving for the four components of coupling coefficients instead of two.

Diameters of the Q circles have been determined understanding that a detuned point lies diametrically opposite a resonant point for any Q circle, i.e.,

$$\text{diameter of } Q \text{ circle} = \left| a_2 - \frac{a_1}{a_3} \right|.$$

Hence, the diameter of the transmission S_{21} Q circle can be described as

$$\text{diameter of } S_{21}\ Q \text{ circle} = \frac{2R_o R_c\,|Y_{\text{ex1}}|\,|Y_{\text{ex2}}|}{(1+\beta_1+\beta_2)} \tag{26}$$

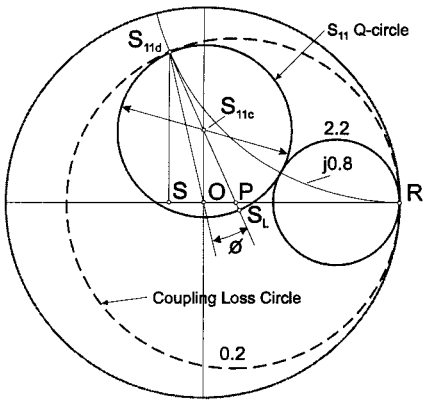

Fig. 12. S_{11} Q circle and coupling loss circle based on [4].

and diameters of the reflection (S_{11} or S_{22}) Q circles are

$$\text{diameter of } S_{pp}\ Q \text{ circle} = \left| \frac{2R_o R_c Y_{\text{exp}}^2}{(1+\beta_1+\beta_2)} \right| = \frac{2R_o R_c\,|Y_{\text{exp}}|^2}{(1+\beta_1+\beta_2)}. \tag{27}$$

By substituting (4) into (26) and (27) and knowing the form of the lossless part of the coupling coefficient described by (24), the diameters of the transmission and reflection Q circles have been expressed in terms of the coupling coefficients as

$$\text{diameter of } S_{21}\ Q \text{ circle} = \frac{2\sqrt{\beta_{1i}}\sqrt{\beta_{2i}}}{1+\beta_1+\beta_2} \tag{28}$$

$$\text{diameter of } S_{11}\ Q \text{ circle} = \frac{2\beta_{1i}}{1+\beta_1+\beta_2} \tag{29}$$

$$\text{diameter of } S_{22}\ Q \text{ circle} = \frac{2\beta_{2i}}{1+\beta_1+\beta_2}. \tag{30}$$

The relationship of the coupling-loss circles to the coupling coefficients, following [4], is illustrated in Fig. 12 for port 1 of the resonator. For an ideal case, when observations are made at the real input of the resonator (point R), the associated coupling loss circle can be visualized as a constant resistance circle that passes through the detuned reflection point S_{11d} of the S_{11} Q circle and the point $R = 1 + j0$ on the Smith chart. The diameter of the coupling loss circle can be found as

$$(\text{diameter of loss circle})|_{\text{port } p} = \frac{1 - |S_{ppd}|^2}{1 - |S_{ppd}|\cos\phi} \tag{31}$$

where ϕ is the angle between the vectors $\overrightarrow{S_{ppd}O}$ and $\overrightarrow{S_{ppd}S_{ppc}}$, where S_{ppd} is the detuned point and S_{ppc} represents the center of the respective Q circle.

To obtain the equations relating the diameters of the coupling-loss circles to the lossless and lossy parts of the coupling coefficients, one needs to consider that the equation for the diameter of the coupling-loss circle at port p is

$$d_p = \frac{2}{1 + \dfrac{R_{sp}}{R_c}} \tag{32}$$

and that based on (25) and (26)

$$\frac{R_{sp}}{R_c} = \frac{g_{epL}}{g_{epi}} = \frac{\beta_{pL}}{\beta_{pi}}. \tag{33}$$

Hence, the diameter of the coupling loss circle can be obtained as

$$d_p = \frac{2}{1 + \dfrac{\beta_{pL}}{\beta_{pi}}}. \tag{34}$$

Solving (29), (30) and (34) for coupling coefficients β_{1i}, β_{1L}, β_{2i}, and β_{2L} yield the following expressions:

$$\begin{aligned}
\beta_{1i} &= \frac{x}{2\left[1 - \left(\dfrac{x}{d_1} + \dfrac{y}{d_2}\right)\right]} \\
\beta_{1L} &= \left(\frac{2}{d_1} - 1\right)\beta_{1i} \\
\beta_{2i} &= \frac{y}{2\left[1 - \left(\dfrac{x}{d_1} + \dfrac{y}{d_2}\right)\right]} \\
\beta_{2L} &= \left(\frac{2}{d_2} - 1\right)\beta_{2i}
\end{aligned} \tag{35}$$

where d_1 is a diameter of the port 1 coupling-loss circle, d_2 is a diameter of the port 2 coupling-loss circle, x is a diameter of the port 1 (S_{11}) Q circle, and y is a diameter of the port 2 (S_{22}) Q circle.

Using the equations derived in this paper, the values of the coupling coefficients and the loaded Q_L factor of a transmission-mode dielectric resonator can be obtained from data sets of S_{11}, S_{22}, and S_{21} measured around the resonance and by applying curve-fitting procedures.

IV. Assessment of the Accuracy of the Transmission-Mode Q_o-Factor Technique Using Computer Simulations

To assess the accuracy of the presented Q-factor measurement technique, several computer simulations have been performed. The transmision-mode Q-factor (TMQF) technique was first applied to ideal Q-circle data sets. Applying the $Q_{\rm Fit}$ software implementation of the developed technique to the ideal S-parameter data sets yielded perfect recovery of the unloaded Q factor. The TMQF technique was next applied to Q circles influenced by noise, electrical delay of transmission lines, coupling losses, and coupling reactances. Q-circle test sets were generated using the software $Q_{\rm Gen}$ [16]. By applying the TMQF procedure to each Q-circle test set, the obtained values of unloaded Q_o factor, loaded Q_L factor, and coupling coefficients results were compared to the nominal values for the test. Simulations were done for Q factors of 9000 and 10 000, similar to values of sapphire dielectric resonators used for verification of the TMQF technique in Section V.

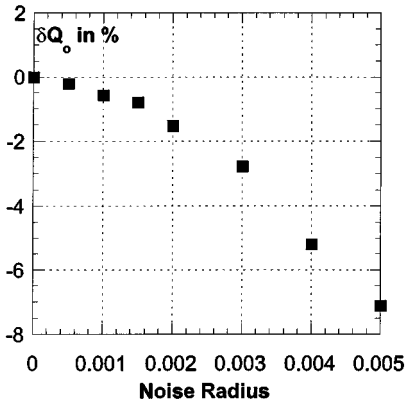

Fig. 13. Calculated error in Q_o from Q_L of S_{21} fit versus noise radius for Q_o of 9000.

A. Investigation of Noise Influence on the Unloaded Q_o Factor Obtained From the TMQF Technique

The effect of noise on the TMQF technique was investigated over a range of noise levels from 0.0005 to 0.005, equivalent to a SNR from 45 to 23 dB. The simulations were performed for the worst-case condition where the same noise was added to all three parameters S_{21}, S_{11}, and S_{22} for each noise level tested. To set the location of the Q circles on the complex plane in positions typical for a practical case, the following parameters of the circuit model of the resonator system of Fig. 10 were used:

1) coupling-loss resistances $R_{s1} = R_{s2} = 5\,\Omega$;
2) coupling reactances $X_{s1} = X_{s2} = 20\,\Omega$;
3) shunt resistance of the ideal resonator $R_o = 5\,\Omega$;
4) source resistance $R_c = 50\,\Omega$;
5) transmission line to wavelength ratio $L/\lambda = 0$;
6) unloaded Q_o factor $= 9000$, $f_o = 10$ GHz;
7) coupling coefficients $\beta_1 = \beta_2 = 0.080$, $N = 401$ points;
8) noise radius ranging from 0.0005 to 0.005.

In the simulation, equal couplings on both ports were used and the frequency span of all Q circles was chosen to be six times the loaded Q bandwidth centered about the resonant frequency. Simulated Gaussian noise data sets were generated using MATLAB V5.3 [19] and the random noise was superimposed on noise-free S-parameter data. Ten independent simulations were performed for each noise level investigated. The $Q_{\rm Fit}$ program was applied to each of the Q-circle test sets (S_{21}, S_{11}, and S_{22}) to calculate the loaded Q_L factor, the coupling coefficients, and the unloaded Q_o factor. The difference between the ideal and calculated Q-factor values is shown in Fig. 13. The simulation results show that the transmission-mode Q_o factor technique can be used to obtain the unloaded Q_o factor from relatively noisy synthesized S-parameter trace data (up to a noise radius of 0.004) with error not exceeding 5%. In many practical measurements performed by the authors, the noise radius did not exceed 0.001. For this value of noise radius, the simulated error of the TMQF technique is better than 0.6%.

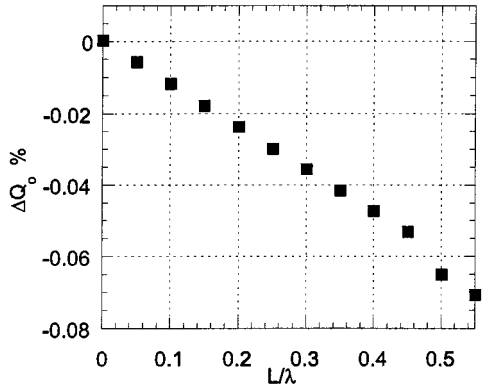

Fig. 14. Calculated error in Q_o using Q_L of the S_{21} fit for Q_o of 10 000.

B. Investigation of Cable Influence on the Unloaded Q_o Factor Obtained From the TMQF Technique

Errors in the calculations of the unloaded Q_o factor due to delay introduced by transmission lines when using the TMQF technique were investigated for short and long transmission lines. For investigations of the effect of delay, the following parameters were selected to simulate the equal coupling condition ($\beta_1 = \beta_2 = 0.08$) and to place the Q circles in positions typical for practical measurements on the complex plane:

1) $R_{s1} = R_{s2} = 5\ \Omega$;
2) $R_{s1} = R_{s2} = 5\ \Omega$;
3) $X_{s1} = X_{s2} = 20\ \Omega$;
4) $R_o = 5\ \Omega$;
5) $R_c = 50\ \Omega$;
6) $N = 401$ points.

The simulations were performed for short and long cable lengths L. For the short cables, the analysis was done for the L/λ ratio varying from 0 to 0.55λ; for the long cable, the analysis was for one case, namely, $L/\lambda = 30$.

Errors in the Q_o factor calculated using the TMQF technique for transmission-line length L/λ from 0 to 0.55 are shown in Fig. 14. The error in the calculated Q_o value increases from 0% to 0.07% with the increase of the line length. The difference in the set and calculated values of the Q_o factors result mostly from errors in the coupling coefficients' calculations, as errors in the Q_L-factor values obtained from the S_{21} fit are below 0.000 03%.

Simulations of the TMQF technique with cables 30 wavelengths long connected on each side of the resonator resulted in the fitted Q_o of 9677, as compared to the actual value of 10 000. The error in for this case was -3.23%.

V. Measurements of the Q Factor of Dielectric Resonators Using the Transmission-Mode Q_o-Factor Technique

To verify applicability of the TMQF technique under differing measurement conditions, the technique has been used for measurements of dielectric resonators of differing values of the Q factor. The measurements were performed on a 10-GHz sapphire resonator with a copper cavity and copper endplates at room temperature of the Q_o factor of 8400, 10-GHz sapphire resonator with a copper cavity and superconducting endplates at cryogenic temperatures with Q_o factors ranging from 8400 to 1 000 000; 25-GHz sapphire resonator with a silver-plated cavity and superconducting endplates with a Q_o factor of 6000 to 300 000, a 17-GHz rexolite resonator with a copper cavity and superconducting endplates of the Q_o factor ranging from 4500 to 10 000; 19-GHz Teflon resonator with copper cavity and superconductor endplates at a cryogenic temperature of the Q_o factor of 63 000–190 000; 17.6-GHz polyethylene resonator with copper cavity and superconducting endplates at a cryogenic temperature of the Q_o factor of 10 000–20 000; 18-GHz strontium–lanthanum–aluminate resonator at room temperature with copper cavity and copper endplates of the Q_o factor of 4560. Measurements of the surface resistance of high-temperature superconductors (HTSs) in a 25-GHz sapphire resonator of the Q factor of approximately 420 000 using the TMQF technique were presented in [16] and [17].

For the verification of the TMQF technique in this paper, we have chosen a resonator with the Q factor of approximately 8400. Measurements of a small Q factor are more difficult than of a large Q-factor value, hence, the verification performed for the small value allows to draw more general conclusions. Measured data and subsequent processing steps using the TMQF technique for the 10-GHz sapphire resonator in a copper cavity at room temperature are presented in Section V-A. The verification measurement system consisted of a chosen resonator, an HP 8722C Vector Network Analyzer, APD DE204SL closed-cycle cryocooler system, two 60-cm low-loss semirigid cables (each cable terminated with a coupling loop), Neocera LTC-10 temperature controller fitted with a 50-W resistive heating element, two silicon diodes temperature sensors, and an IBM-PC computer.

A. Verification of the TMQF Technique for the Resonator With the Q_o Factor of 8400

The resonator chosen for verification contained a sapphire rod of 7.41-mm height and 12.3 2-mm diameter enclosed in the copper cavity of 24-mm diameter [18]. The geometrical factors of the resonator were $A_m = 27617$, $A_s = 279$, $p_e = 0.971$, and $\epsilon_r = 9.38$. The sapphire rod was assumed to have $\tan\delta$ of 5×10^{-8}. The measurements were performed with microwave source power of -15 dBm.

The 10-GHz sapphire resonator with moderate coupling had the insertion loss at a resonance of -20.8 dB. Between 579–1601 measurement points around the resonance were logged for each of the scattering parameters S_{21}, S_{11}, and S_{22}. Figs. 15 and 16 present raw measurement data and Figs. 17–20 give step-by-step correction of data using the transmission-mode Q_o-factor technique.

In Fig. 15, 1601 points representing S_{21} values measured with the vector network analyzer, as well as the fitted circle obtained using the basic TMQF technique are shown. The curve fit implemented in the $Q_{\rm Fit}$ software of the TMQF technique [16] resulted in a loaded Q_L factor of 7393 and a resonant frequency of 9.924949 GHz. The SNR of the trace was high (46.7 dB) and the trace was not "contaminated" by the frequency dependence

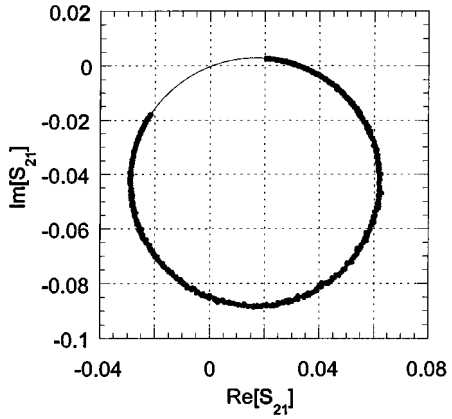

Fig. 15. Measured S_{21} data with 1601 points spanning 5 MHz and a fitted S_{21} Q circle.

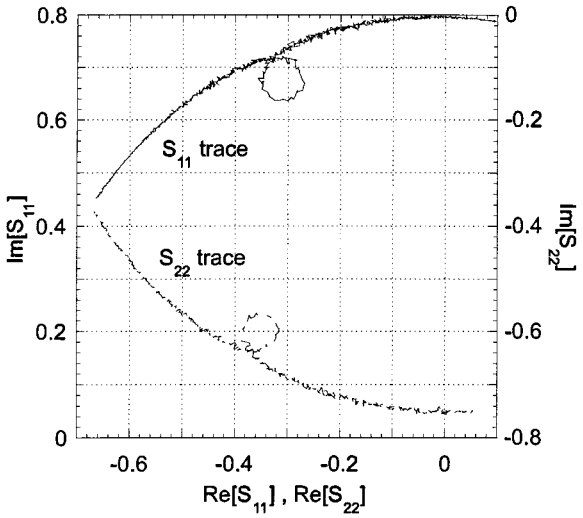

Fig. 16. Measured S_{11} data and S_{22} data including off-resonance regions.

of delay; hence, no further processing of S_{21} was necessary. The SNR was calculated as follows:

$$\mathrm{SNR}_{dB} = 20\log_{10}\frac{R}{\sqrt{\dfrac{1}{N}\displaystyle\sum_{i=1}^{N}(R-r_i)^2}} \tag{36}$$

where R is the radius of the Q circle and r_i is the magnitude of the ith point of the N point S-parameter data set obtained from measurements around the resonance.

Fig. 16(a) and (b) shows measured reflection S_{11} and S_{22} traces containing 710 and 579 points, respectively. Wide measurement spans of 44.3 and 36.1 MHz were used to obtain the resonant circles, as well as significant parts of the off resonance circles so that the correction of the impedance mismatch and the phase distortion of the S_{11}- and S_{22}-parameters could be performed. To improve resolution and SNR in the resonant circles, narrow span measurements would be better. However, it would have required taking measurements of S_{11} and S_{22} data twice. Hence, it is more economical to take S_{11} and S_{22} measurements in wide span as noise is removed from the data through the curve-fitting procedure. The SNR of S_{11} and S_{22} traces were 22.9 and 23.6 dB, respectively.

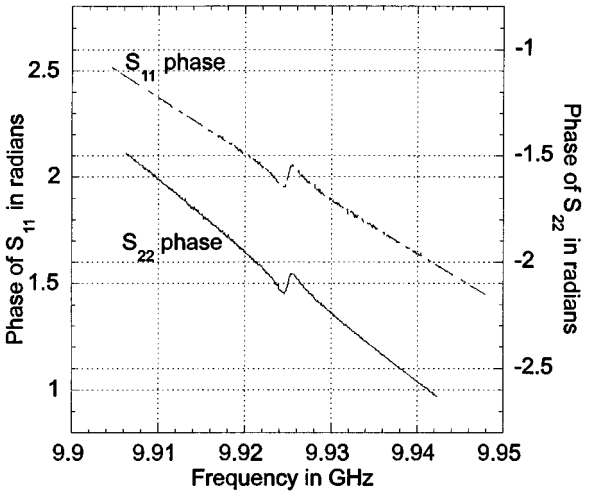

Fig. 17. Phase of S_{11} and of S_{22} versus frequency over a wide bandwith.

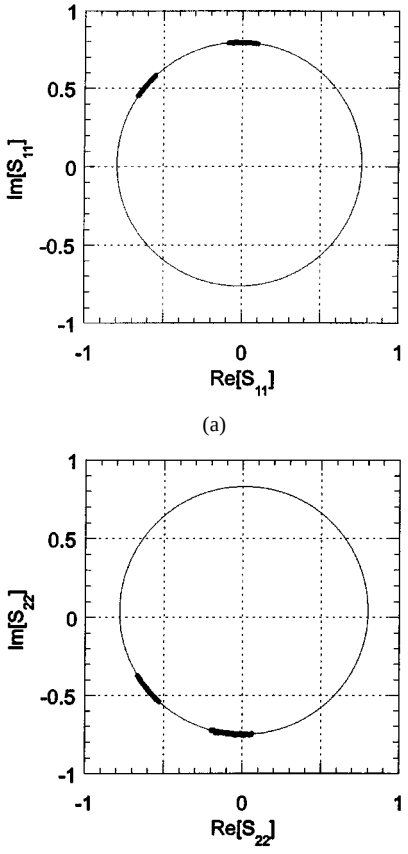

Fig. 18. Reconstructed off resonance circles of: (a) S_{11}- and (b) S_{22}-parameters.

The reflection traces in Fig. 16 are clearly distorted due to impedance mismatch resulting in shift of the circles from their ideal locations. Center coordinates for the S_{11} circle are 0.01593 and 0.01669 with a radius of 1.559. For the S_{22} circle, coordinates of the center are 0.00776 and 0.03976 with a radius of 1.5812. Phase distortion is also present due to uncalibrated cables, and this is visible in Fig. 17, presenting the phase of S_{11}

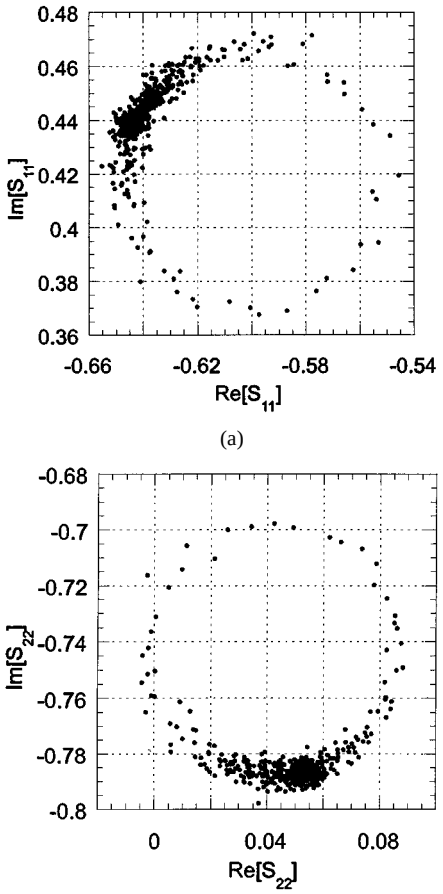

Fig. 19. Phase corrected: (a) S_{11} Q circle with 710 points and a span of 44.3 MHz and (b) S_{22} Q circle with 579 points and a span of 36.1 MHz.

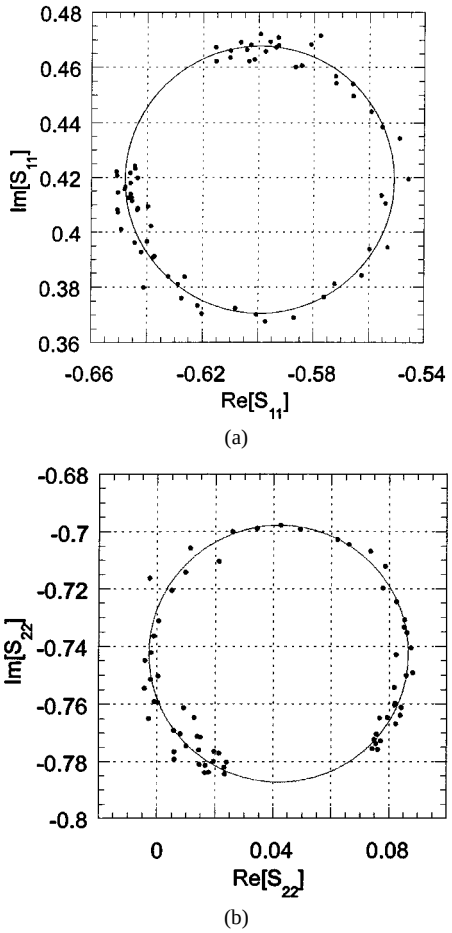

Fig. 20. Pruned phase corrected: (a) S_{11} Q circle and (b) S_{22} circle.

and S_{22} versus frequency. Both distortions need to be removed from the measurement data before coupling coefficients may be calculated.

The linear fits of the wide span S_{11} and S_{22} phase data of Fig. 17 give the rate of change in phase of -2.459×10^{-8} rad/Hz. and -3.161×10^{-8} rad/Hz, respectively. These values of the phase rate were used to correct the S_{11} and S_{22} resonance circles. The off-resonance traces of Fig. 16 allowed for the reconstruction of the off resonance circles and for compensation for the offset, as shown in Fig. 18.

The phase and mismatch corrected resonant S_{11} and S_{22} circles are shown in Fig. 19. As can be seen the corrected reflection, resonant circles contain a large concentration of points around the detuned regions, which would cause a heavy bias in the fitting procedure. To remove the influence of the detuned regions, the end sections of the S_{11} and S_{22} Q circles are deleted.

Fig. 20 shows reduced data sets of the corrected S_{11} (71 points, span $=$ 4.375 MHz) and S_{22} Q circles (66 points, span $=$ 4.063 MHz) and the resulting fitted circles. Using the procedure described in Section III-B and the results shown in Fig. 20, the coupling coefficient β_1 and β_2 of 0.061 and 0.056, respectively, were obtained. The lossless and lossy parts of β_1 and β_2 were equal to 0.0544 and 0.0069 and 0.049 96 and 0.0059, respectively.

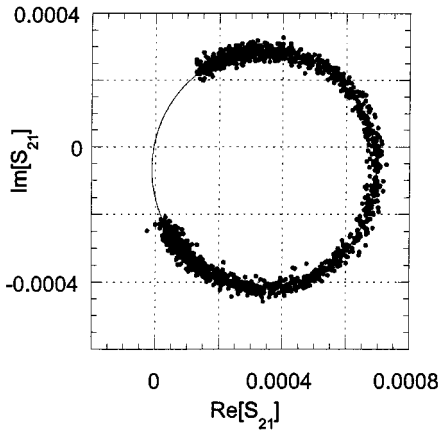

Fig. 21. Measured 1601 points S_{21} and fitted S_{21} Q circle for the case of very weak coupling with a 3-MHz span.

Using the computed values of the coupling coefficients and loaded Q factor, the unloaded Q factor Q_o of 8258.3 was obtained.

The same 10-GHz resonator was measured with a very weak coupling since the Q_o factor can be approximated by the loaded Q_L factor ($Q_o \approx Q_L|_{\beta_1\approx\beta_2\approx0}$). The measured S_{21} trace is shown in Fig. 21 with 1601 points spanning 3 MHz. The resulting insertion loss at resonance was -63 dB and the SNR ratio for the S_{21} trace was 28.2 dB. Under this weak coupling, the S_{11} and S_{22} reflection Q circles were too small to be seen

TABLE II
Q-FACTORS OF VARIOUS RESONATORS MEASURED USING THE TMQF TECHNIQUE

Frequency in GHz	Dielectric	Endwall Material	Qo-Factor
10	sapphire	superconductor	8,400 - 1,000,000
17	rexolite	superconductor	4,500 - 10,000
17.6	polyethylene	superconductor	10,000 - 20,000
18	strontium lanthanum aluminate	copper	4,560
19	teflon	superconductor	63,000 - 190,000
25	sapphire	superconductor	420,000

even with the highest resolution. The data scatter D_s for the S_{21} trace was calculated to be 0.072, which did not exceed the recommended limit of 0.1 for reliable results. Hence, the circle-fitting procedure provides reliable fit results without any further processing.

Using the TMQF fitting procedure, the loaded Q_L factor (and, hence, the Q_o factor) of 8382 was obtained. Fitted resonant frequency was 9.924136 GHz. The difference between the unloaded Q_o factor obtained from the measurements under very weak coupling (IL $= -63$ dB) and the moderate coupling (IL $= -20.8$ dB) was only -1.5%. This good agreement of the Q_o-factor values for two very different couplings shows the high accuracy of the developed TMQF technique for unloaded Q_o-factor measurements under the influence of noise, transmission line delay, and coupling losses and reactances.

Apart from measurements presented above, we performed tests of dielectric resonators with various Q-factor values, as listed in Table II.

VI. CONCLUSIONS

The presented transmission-mode Q-factor technique has proven to be a reliable tool for accurate measurements of the unloaded Q_o factor of microwave resonators in the presence of noise, uncalibrated cables and connectors, impedance mismatch, crosstalk, and coupling loss. Computer simulations have shown that the addition of noise with a noise radius below 0.001 results in an error smaller than 0.6% in calculated values of the Q_o factor for the nominal value of 9000. Simulations with uncalibrated cables added resulted in errors of 0.07% for two cables 0.55 wavelengths long and -3.3% for two cables 30 wavelengths long. The error in the Q_o-factor calculations due to the uncalibrated cables using the TMQF technique decreases as the Q increases by the same factor.

Measurements of the 10-GHz dielectric resonator with the Q_o factor of the order of 9000 at a very low coupling and at a moderate coupling resulted in a difference of only 1.5%. We have applied the developed method to several Q_o measurements of sapphire, rexolite, strontium–lanthanum–aluminate ($SrLaAlO_4$) (SLA), Teflon, and polyethylene resonators in the range from 4560 to 1 000 000 at cryogenic temperatures and have found the performance very satisfactory. In general, we conclude that the TMQF technique can be applied for the Q-factor measurements above 1000.

ACKNOWLEDGMENT

The authors would like to acknowledge D. Kajfez, University of Mississippi, University, and J. Krupka, Politechnika Warszawska, Warsaw, Poland, for inspiring our research, C. Wilker, DuPont Superconductivity, Wilmington, DE, for discussions on the final version of this paper's manuscript, and G. Allen, James Cook University, Townsville, Qld., Australia, and R. McTaggart, James Cook University, Townsville, Qld., Australia, for help with the editing of this paper's manuscript.

REFERENCES

[1] R. Woode, M. Tobar, and E. Ivanov, "An ultralow noise microwave oscillator based on a high-Q liquid nitrogen cooled sapphire resonator," *IEEE Trans. Ultrason., Ferroelect., Freq. Contr.*, vol. 43, pp. 936–1996, Sept. 1996.

[2] C. Wilker, Z.-Y. Shen, V. X. Nguyen, and M. S. Brenner, "A sapphire resonator for microwave characterization of superconducting thin films," *IEEE Trans. Appl. Superconduct.*, vol. 3, pp. 1457–1460, Mar. 1993.

[3] J. Krupka, K. Derzakowski, M. E. Tobar, J. Hartnett, and R. G. Geyer, "Complex permittivity of some ultralow loss dielectric crystals at cryogenic temperatures," *Meas. Sci. Technol.*, vol. 10, pp. 387–392, Oct. 1999.

[4] D. Kajfez, *Q Factor*. University, MS: Vector Fields, 1994.

[5] E. L. Ginzton, *Microwave Measurements*. New York: McGraw-Hill, 1957, pp. 403–408.

[6] E. J. Vanzura and J. E. Rogers, "Resonant circuit model evaluation using reflected S-parameter data," in *Proc. IEEE Instrum. Meas. Technol. Conf.*, Atlanta, GA, May 14–16, 1991, pp. 150–155.

[7] J. Wosik, L. M. Xie, K. Nesteruk, D. Li, J. H. Miller, Jr., and S. A. Long, "Power handling capabilities of superconducting YBCO thin films: Thermally induced nonlinearity effects," *J. Superconduct.*, vol. 10, no. 2, p. 97, 1997.

[8] T. Miura, T. Takahashi, and M. Kobayashi, "Accurate Q factor evaluation by resonance curve area method and it's application to the cavity perturbation," *IEICE Trans. Electron.*, vol. E77-C, no. 6, pp. 900–907, June 1994.

[9] M. C. Sanchez, E. Martin, and J. M. Zamarro, "Unified and simplified treatment of techniques for characterizing transmission, reflection, or absorption resonators," *Proc. Inst. Elect. Eng.*, pt. H, vol. 137, no. 4, pp. 209–212, Aug. 1990.

[10] M. C. Sanchez *et al.*, "New method for the measurement of coupling coefficients of transmission cavities," *Proc. Inst. Elect. Eng.*, pt. H, vol. 134, no. 1, pp. 103–105, Feb. 1987.

[11] Z. Ma, "RF properties of high temperature superconducting materials," Ph.D. dissertation, Edward L. Ginzton Lab., Stanford Univ., Stanford, CA, 1995.

[12] D. Kajfez, "Linear fractional curve fitting for measurement of high Q factors," *IEEE Trans. Microwave Theory Tech.*, vol. 42, pp. 1149–1153, July 1994.

[13] A. L. Luiten, A. G. Mann, and D. G. Blair, "High-resolution measurement of the temperature-dependence of the Q, coupling and resonant frequency of a microwave resonator," *Meas. Sci. Technol.*, vol. 7, no. 6, pp. 949–949, 1996.

[14] A. P. S. Khanna and Y. Garault, "Determination of loaded, unloaded and external quality factors of a dielectric resonator coupled to a microstripline," *IEEE Trans. Microwave Theory Tech.*, vol. MTT-31, pp. 261–264, Mar. 1983.

[15] J. E. Aitken, "Swept-frequency microwave Q factor measurements with network analyzer," *Proc. Inst. Elect. Eng.*, vol. 123, pp. 855–862, 1976.

[16] K. Leong, "Precise measurements of surface resistance of HTS thin films using a novel method of Q-factor computations for sapphire dielectric resonators in the transmission mode," Ph.D. dissertation, Dept. Elect. Eng., James Cook Univ., Townsville, Qld., Australia, 2000.

[17] K. Leong and J. Mazierska, "Accurate measurements of surface resistance of HTS films using a novel transmission mode Q factor technique," *J. Superconduct.*, vol. 14, no. 1, pp. 93–103, 2001.
[18] J. Mazierska, "Dielectric resonator as a possible standard for characterization of high temperature superconducting films for microwave applications," *J. Superconduct.*, vol. 10, no. 2, pp. 73–85, 1997.
[19] *MATLAB Users Guide*, Math Works, Natick, MA, 1989.

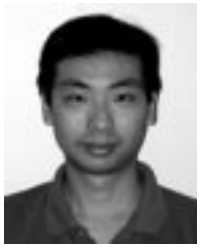

Kenneth Leong (S'91–M'92) was born in Townsville, Qld., Australia, in 1969. He received the B.Eng. degree (with honors) and Ph.D. degree in electrical engineering from the James Cook University, Townsville, Qld., Australia, in 1994 and 2000, respectively.

From January 2000 to December 2001, he was been a Research Officer with the Electrical and Computer Engineering, James Cook University, where he was involved with microwave measurements of materials including high-temperature superconducting thin films and dielectrics for applications in wireless communications. He developed a precise method of Q-factor computations for dielectric resonators working in the transmission mode. This method, known as the transmission-mode Q-factor technique, is utilized at the James Cook University for accurate measurements of the surface resistance of HTS films and loss tangent of dielectric materials. Since February 2002, he has been a Visiting Post-Doctoral Researcher with the Electromagnetic Technology Division, National Institute of Standards and Technology (NIST), Boulder, CO, where he is involved with the high T_c Electronics Project.

Dr. Leong is a member of the IEEE Microwave Theory and Techniques Society (IEEE MTT-S). He was the recipient of the 1997 Third Best Student Paper Prize presented at the MTT-S International Microwave Symposium (IMS), Denver, CO, and the 1994 Best Honors Presentation Prize presented by the Faculty of Engineering, James Cook University.

Janina Mazierska (SM'83) received the M.S.E.E. and Ph.D. degrees in electronic engineering from the Warsaw University of Technology, Warsaw, Poland, in 1970 and 1979, respectively.

From 1972 to 1982, she was with the Institute of Electronic Fundamentals, Warsaw University of Technology, where she specialized in modeling of fast semiconductor devices for computer-aided design of pulse and microwave circuits. From 1983 to 1987, she was on an assignment with the Department of Physics, University of Jos, Jos, Nigeria, under a Polish–Nigerian inter-governmental agreement. During this time, she assisted in the development of an electronics/applied physics degree. Since 1987, she has been with the James Cook University, Townsville, Qld., Australia, where she is currently an Associate Professor of electrical and computer engineering. In 1991 and 1996, she was a Visiting Scholar with the Ginzton Laboratory, Stanford University. She has authored or coauthored 96 papers and conference presentations. Her current research interests are microwave properties of HTSs and dielectric materials for applications in wireless communication systems.

Dr. Mazierska is chair of the IEEE Microwave Theory and Techniques Society (IEEE MTT-S)/Comm Joint Chapter and a member of the IEEE MTT-S Transnational Committee, the IEEE Prize Papers/Scholarship Awards Committee, and the IEEE Meeting and Services Committee. She is a Region 10 conference coordinator and a North Queensland Section vice-chair.